

# Unexpected metabolic rewiring of CO<sub>2</sub> fixation in H<sub>2</sub>-mediated materials-biology hybrids

Yongchao Xie<sup>1</sup>, Sevcan Erşan<sup>2</sup>, Xun Guan<sup>1</sup>, Jingyu Wang<sup>1</sup>, Jihui Sha<sup>3</sup>, Shuangning Xu<sup>1</sup>, James A. Wohlschlegel<sup>3</sup>, Junyoung O. Park<sup>2,4</sup>, Chong Liu<sup>1,4,\*</sup>

<sup>1</sup> Department of Chemistry and Biochemistry, University of California Los Angeles, Los Angeles, California 90095, United States.

<sup>2</sup> Department of Chemical and Biomolecular Engineering, University of California Los Angeles, Los Angeles, California 90095, United States.

<sup>3</sup> Department of Biological Chemistry, University of California Los Angeles, Los Angeles, California 90095, United States.

<sup>4</sup> California NanoSystems Institute, University of California Los Angeles, Los Angeles, California 90095, United States.

\* Corresponding author: Chong Liu

Email: chongliu@chem.ucla.edu

## Author contributions:

Y.X. conceptualized the project, developed the hybrid systems and conducted the majority of the experiments; S.E. and Y.X. conducted the metabolomic experiments and data analysis under the supervision of J.O.P.; X.G. helped establish the electrochemical setup; J.W. conducted the scanning electron microscopy characterizations; S.X. contributed to the NMR analysis; J.S. and Y.X. conducted the proteomic experiments and data analysis under the supervision of J.A.W.; Y.X. wrote the first draft of the manuscript; C.L. supervised the project; All authors provided input and edits to the final manuscript.

## Competing interests:

The authors declare no competing financial interest.

## Classification:

Physical Sciences – Chemistry; Biological Sciences – Sustainability Science

**Keywords**

Materials-biology hybrid, CO<sub>2</sub> fixation, metabolic rewiring, proteomics, metabolomics.

**This PDF file includes:**

Main Text

Figures 1 to 4

## Abstract

A hybrid approach combining water-splitting electrochemistry and H<sub>2</sub>-oxidizing, CO<sub>2</sub>-fixing microorganisms offers a viable solution of producing value-added chemicals from sunlight, water, and air. The classic wisdom without thorough examination to date assumes that the electrochemistry in such a H<sub>2</sub>-mediated process is innocent of altering microbial behavior. Here we report unexpected metabolic rewiring induced by water-splitting electrochemistry in H<sub>2</sub>-oxidizing acetogenic bacterium *Sporomusa ovata* that challenges such a classic view. We found that the planktonic *S. ovata* is more efficient in utilizing reducing equivalent for ATP generation and hence CO<sub>2</sub> fixation in the materials-biology hybrids, supported by our metabolomic and proteomic studies. These observations unravel previously underappreciated materials' impact on microbial metabolism in seemingly simply H<sub>2</sub>-mediated charge transfer between biotic and abiotic components. Such a deeper understanding at the materials-biology interface will foster advanced design of hybrid systems for sustainable chemical transformation.

## Significance Statement

The use of renewable electric energy to power material-microbe hybrids for chemical synthesis has emerged as a promising approach for a sustainable society. When the materials and microbes are not in physical contact with each other, it is commonly assumed that the materials component that facilitates an electron transfer mediated by redox molecules such as H<sub>2</sub> does not serve to perturb microbial metabolism significantly. However, this study revealed that the electrochemical system can induce a fortuitous metabolic rewiring in planktonic *S. ovata* cells, which differs from what was previously assumed. This observation underscores the importance of revisiting existing assumptions of materials-biology interaction and adopting a more holistic approach to understand the underlying mechanisms at material-microbe interfaces.

## Keywords

Materials-biology hybrid, CO<sub>2</sub> fixation, metabolic rewiring, proteomics, metabolomics.

## Main Text

### Introduction

The hybrid approach that integrates microbial catalysts with synthetic electrocatalysis has gained momentum in recent years for a variety of chemical transformations in the context of a sustainable future (1-6). Potentially powered by renewable energy such as solar electricity, such bioelectrochemical materials-biology hybrids have been deployed for the sustainable production of valuable commodity chemicals (7-9) and efficient remediation of environmental pollutants (10-12). In those systems, the material components serve as the sole electron donor and transduce electricity to chemical driving forces powering microbial metabolisms for desired applications under the electroautotrophic conditions (10, 13). The materials' efficient charge transfer and the microbes' synthetic versatility and selectivity synergistically coalesce at the materials-biology interactions, leading to high efficiencies and reaction throughput for challenging chemical transformations such as the fixation of CO<sub>2</sub> and N<sub>2</sub> (5, 14-19). Hence a detailed understanding of the mutual interactions between the biotic and abiotic components (20-22) is of critical importance for the development of sustainable techniques addressing the challenges that our society is facing.

The conventional wisdom of the materials-biology hybrids assumes that while a direct physical contact of the biotic and abiotic components may affect beneficial synergies on both components (3, 6, 13), an indirect charge transfer via mediated redox couple may lead to minute if any changes on individual components' functionality. Indeed, in the research of bioelectrochemical fixation of CO<sub>2</sub> when H<sub>2</sub> generated by electrochemical proton reduction is the mediating redox species (23, 24), H<sub>2</sub>-oxidizing chemolithotrophic *Ralstonia eutropha* (7, 25, 26), diazotrophic *Xanthobacter autotrophicus* (8, 14, 27), methanogenic *Methanosarcina barkeri* (28, 29), and acetogenic *Sporomusa ovata* (15, 30-34) were readily plugged into water-splitting electrocatalytic systems assuming no metabolomic responses and gene regulations due to the perceived indirect charge transfer in the hybrids. However, the hypothesized invariance of microbial metabolism in those H<sub>2</sub>-mediated electroautotrophic systems has not been tested. As recent studies at the physical interface between light-absorbing semiconductors and CO<sub>2</sub>-fixing organisms uncover unexpected material-induced metabolomic modulation (16, 35), the potential risk of understating metabolic rewiring in materials-biology hybrids with indirect charge transfer looms large, due to the absence of a thorough examination of microbial metabolism in those systems. A detailed, appropriate understanding of how microbial metabolism responds to materials'

presence in H<sub>2</sub>-mediated electroautotrophic systems will facilitate the design and development of advanced hybrids in the future.

We aim to rigorously test the hypothesized invariance of microbial metabolism in H<sub>2</sub>-mediated materials-biology hybrids, hence shed more lights on the fundamental interactions between the abiotic and biotic components during the mediated indirect charge transfer (Fig. 1A). Built upon our previous experience (7, 14, 15, 31), the model H<sub>2</sub>-mediated hybrid system that we aim to study includes H<sub>2</sub>-oxidizing *S. ovata* for the fixation of CO<sub>2</sub> into acetic acid via the Wood-Ljungdahl pathway (36), as well as biocompatible water-splitting electrocatalysts made of cobalt-phosphorous (Co-P) alloy for hydrogen evolution reaction (HER) (Fig. 1B) (7). Previous studies have established a H<sub>2</sub>-mediated delivery of reducing equivalents from the electrode to planktonic *S. ovata* under sufficiently high water-splitting current densities (31, 37). Yet it remains unknown whether the electrochemical process(es), seemingly innocent and only responsible for H<sub>2</sub> generation, will perturb microbial metabolism beyond the delivery of H<sub>2</sub>.

In this work, we report the unexpected discovery that the seemingly innocent water-splitting electrocatalysis induced observable and significant metabolomic rewiring of planktonic *S. ovata* in the materials-biology hybrids of CO<sub>2</sub> fixation. We found a higher efficiency for microbes to utilize the generated H<sub>2</sub> for CO<sub>2</sub> fixation in the hybrid system, than the one observed when *S. ovata* was cultured chemoautotrophically with externally supplied H<sub>2</sub> under otherwise the same experimental conditions (Fig. 1A). Metabolomic and proteomic studies comparing the electroautotrophic and chemoautotrophic cultures unraveled fortuitous metabolomic rewiring including membrane electrochemical potential regulation and enhanced proton transmembrane transport in the hybrid systems, leading to an increased adenosine triphosphate (ATP) generation and an accelerated rate of CO<sub>2</sub> fixation. Our observations challenged the conventional simple picture of H<sub>2</sub>-mediated indirect charge transfer and suggested the presence of previously underappreciated metabolic impact of inorganic electrodes on microbial catalysts. Such an advance in fundamental understanding at the materials-biology interactions heralds additional design considerations for a sustainable chemical transformation that maximizes the benefits of materials-biology hybrids.

## Results

### Enhanced CO<sub>2</sub> fixation in H<sub>2</sub>-mediated electroautotrophic hybrid

H<sub>2</sub>-mediated bioelectrochemical fixation of CO<sub>2</sub> was established in a two-chamber setup under a flowing gas environment of CO<sub>2</sub>:N<sub>2</sub> (20:80, v:v, 6 mL min<sup>-1</sup>) at 30 °C (Supplementary Fig. S1). In the cathode chamber of such setup, a biocompatible Co-P alloy HER electrocatalysts developed in our previous studies (Fig. 1B, Supplementary Fig. S2A, S2B) (7, 14, 31, 38), composed of a P:Co weight ratio of 1:4.4 as characterized by energy-dispersive X-ray spectroscopy (Supplementary Fig. S2C), was applied to couple with acetogenic bacterium *S. ovata* strain H1 (DSM 2662) (39) for the reduction of CO<sub>2</sub> into acetic acid. Reported to yield H<sub>2</sub> with 100% Faradaic efficiency (38), Co-P alloy is electrocatalytically active for HER at least over 48 hours based on the measured cyclic voltammograms (Fig. 1C) and is known to not inhibit the growth or CO<sub>2</sub> fixation of *S. ovata* (31). The minimal medium deployed in the process does not contain any carbon substrates, except the dissolved bicarbonate (NaHCO<sub>3</sub>), trace vitamin additives, and the minute amounts of cysteine as the reducing reagent (0.2 mM) for an anaerobic solution (Supplementary Note 1). Two-week control experiment inoculated with *S. ovata* in CO<sub>2</sub>:N<sub>2</sub> (20:80, v:v) but without the provision of either H<sub>2</sub> or electrons did not yield observable bacterial growth or acetate accumulation from CO<sub>2</sub> fixation (Supplementary Fig. S3). Hence any observation of bacterial growth or acetate accumulation originates from the provision of H<sub>2</sub> or electrons for CO<sub>2</sub> fixation.

We report that *S. ovata* under electroautotrophic conditions in the bioelectrochemical setup is nearly 100% efficient in utilizing reducing equivalents and fixing CO<sub>2</sub> into acetic acid by repeated independent tests (Supplementary Table S1). Chronoamperometry measurements for the materials-biology hybrid at  $-1.34 \pm 0.10$  mA/cm<sup>2</sup> ( $n = 3$ , same below) equivalent to about  $-0.77$  to  $-0.96$  V vs. standard hydrogen electrode (SHE). In such a flowing CO<sub>2</sub>/N<sub>2</sub> condition, the H<sub>2</sub> supply rate is  $2.40 \pm 0.19$  millimole per day (mmole d<sup>-1</sup>), equivalent to an e<sup>-</sup> supply rate of  $4.80 \pm 0.37$  mmole d<sup>-1</sup>, while the accumulation rate of acetate was determined as  $0.67 \pm 0.08$  mmole d<sup>-1</sup> based on the measurement of <sup>1</sup>H NMR spectroscopy (Entry 1 in Supplementary Table S1). Such an observed level of acetate production rate is at least comparable to our previous report (31) and other reported bioelectrochemical systems deploying acetogens for CO<sub>2</sub> fixation (Supplementary Table S2). In two independent tests, the apparent electron efficiency  $\eta_{\text{app,electro}}$ , or the apparent Faradaic efficiency that describes the percentage of electrons contributing to CO<sub>2</sub> reduction into acetic acid, was calculated to be  $112 \pm 6\%$  and  $110 \pm 9\%$  (Entry 1 and 2 in Supplementary Table S1, respectively), based on the trajectory of acetate accumulation sampled every 24 hours (Fig.

1D). The higher-than-100%  $\eta_{\text{app,electro}}$  is proposed to originate from the residual extracellular oxidizable organics carried over during bacterial inoculation (40), since the chemical oxygen demand (COD) of the extracellular component of the *S. ovata* inoculum at the beginning of experiments was measured to be  $1.99 \pm 0.85$  mmole of electron equivalents. Accounting the contribution of residual extracellular oxidizable organics (Supplementary Fig. S4), the corrected  $e^-$  efficiency of electroautotrophic CO<sub>2</sub> fixation  $\eta_{\text{electro}} = 99 \pm 4\%$  and  $95 \pm 10\%$  in two independent tests (Entry 1 and 2 in Supplementary Table S1, respectively). After the three-day electroautotrophy, the visual inspection did not observe any biofilms on the Co-P cathode's surface, nor did images of scanning electron microscopy, while a small percentage of the electrode surface, on the order of  $0.03 \text{ cell } \mu\text{m}^{-2}$ , includes attached bacterial cells (Supplementary Fig. S5). We estimated that the bacterial cells with direct materials contact, necessary but not sufficiently indicative of a direct electron transfer (41), constitute no more than 0.1% of the predominantly planktonic bacterial cell cultures. Thus our observations support a near-unity of  $e^-$  efficiency for H<sub>2</sub>-mediated materials-biology hybrids of CO<sub>2</sub> fixation.

Surprisingly, the  $e^-$  efficiency is lower for the microbes grown under chemoautotrophic conditions, even though both electroautotrophic and chemoautotrophic conditions utilize H<sub>2</sub> as the direct reductant for the CO<sub>2</sub>-fixing through the Wood-Ljungdahl pathway (36). The headspace of chemoautotrophic *S. ovata* culture was intermittently dosed with mixed gas (H<sub>2</sub>:CO<sub>2</sub>, 80:20, v:v) every 12 hrs including 2 mmole H<sub>2</sub> substrate (i.e.,  $e^-$  supply rate of  $8 \text{ mmole d}^{-1}$ ) whose amount was higher than the ones in bioelectrochemical experiments ( $4.80 \pm 0.37 \text{ mmole } e^- \text{ d}^{-1}$ ). However, based on temporal trajectory of acetate accumulation, the acetate production rate in chemoautotrophic *S. ovata* culture is  $0.48 \pm 0.02 \text{ mmole d}^{-1}$  (Fig. 1E and entry 3 in Supplementary Table S1), which was lower than  $0.67 \pm 0.08 \text{ mmole d}^{-1}$  in electroautotrophic cultures (Entry 1 in Supplementary Table S1). Quantifying H<sub>2</sub> consumption in the headspace via gas chromatography established the mass balance of reducing equivalents and led to the averaged apparent  $e^-$  efficiency  $\eta_{\text{app,chemo}}$  of  $81 \pm 4\%$  (Fig. 1E). The corrected  $e^-$  efficiency  $\eta_{\text{chemo}}$  of  $71 \pm 4\%$  after subtracting the contribution of extracellular carried-over nutrients (see above), is significantly lower than the  $\eta_{\text{electro}}$  of  $99 \pm 4\%$  in the bioelectrochemical case (Entry 1 and 3 in Supplementary Table S1). Meanwhile, a lower protein yield, a good surrogate of biomass accumulation (16, 42), was observed for chemoautotrophic *S. ovata* ( $14.9 \pm 1.0 \mu\text{g protein mL}^{-1}$ ) than the electroautotrophic ones ( $20.9 \pm 2.1 \mu\text{g protein mL}^{-1}$ ) (Supplementary Table S1). Such results suggest that the

electroautotrophic *S. ovata* is more efficient in utilizing reducing equivalent H<sub>2</sub> for the fixation of CO<sub>2</sub> and biomass accumulations.

Additional experiments, originally meant as controls to study the impacts of H<sub>2</sub> delivery conditions, allude to different metabolic conditions between chemoautotrophy and H<sub>2</sub>-mediated electroautotrophy. Instead of intermittently dosing *S. ovata* with 80% H<sub>2</sub> at 1 bar pressure that strongly favors CO<sub>2</sub> fixation thermodynamically (43), we aimed to mimic the mass transport and delivery amount of H<sub>2</sub> in electroautotrophy and conducted chemoautotrophic experiments in the same bioelectrochemical setup, with a continuous gas flow of 1% H<sub>2</sub> (H<sub>2</sub>:CO<sub>2</sub>:N<sub>2</sub>, 1:20:79, v:v:v) whose H<sub>2</sub> mass transport and delivery amount resemble if not replicate the ones in electroautotrophic conditions. Unexpectedly, minimal bacterial CO<sub>2</sub> fixation hence biomass accumulation was observed after multiple attempts (Fig. S6, Entry 5 and 6 in Supplementary Table S1), different from the chemoautotrophic growth under 80% H<sub>2</sub> (Entry 3 and 4 in Supplementary Table S1). Multiple attempts of chemoautotrophic culturing under 1% H<sub>2</sub> in the batch mode, which observed the active bacteria growth under 80% H<sub>2</sub>, also failed to yield detectable bacterial CO<sub>2</sub> fixation (data not shown). These observations suggest that the low H<sub>2</sub> partial pressure (1% H<sub>2</sub>) disfavoring CO<sub>2</sub> fixation thermodynamically (43) has a significant metabolic impedance of chemoautotrophy, despite the fact that robust microbial CO<sub>2</sub> fixation with high e<sup>-</sup> efficiency was observed in electroautotrophy. Our observations lead us to hypothesize that metabolic stimulation and modulation of *S. ovata* are present in the seemingly simple H<sub>2</sub>-mediated electrochemical system, warranting detailed comparative, integrated metabolomic and proteomic studies for a deeper fundamental understanding in the hybrid system.

### **Observed metabolomic shift in planktonic *S. ovata* cells under electroautotrophic conditions**

There are significant metabolic profile differences between the electroautotrophic and chemoautotrophic planktonic *S. ovata*. To understand the difference, we extracted and measured intracellular metabolites with triplicates ( $n = 3$ ) from the electroautotrophic and chemoautotrophic cultures. Since chemoautotrophic *S. ovata* under 1% H<sub>2</sub> in the bioelectrochemical setup were not active in acetate production, only *S. ovata* active of CO<sub>2</sub> fixation under electroautotrophic and chemoautotrophic conditions with 80% H<sub>2</sub> were collected for subsequent metabolomic and proteomic analyses (Entry 1 and 4 in Supplementary Table S1, respectively). Out of more than 400 intracellular metabolites involving the majority of metabolic pathways that we searched for, a



total of 118 metabolites were measured in both electroautotrophic and chemoautotrophic cultures and 11 metabolites were exclusively detected in electroautotrophic one (Supplementary Table S3). The visualization of the principal component analysis (PCA) with the first two components (Fig. 2A), accounting for a combined 77.7% of variance, distinguishes the metabolomes extracted from cells under electroautotrophic and chemoautotrophic conditions.

Our metabolomic study suggests increased redox cofactor pools in the materials-biology hybrids for CO<sub>2</sub> fixation. The redox cofactors including nicotinamide adenine dinucleotide in both oxidized (NAD<sup>+</sup>) and reduced (NADH) forms, and oxidized nicotinamide adenine dinucleotide phosphate (NADP<sup>+</sup>) all display higher abundance in *S. ovata* cells grown bioelectrochemically, while the concentration ratio between NADH and NAD<sup>+</sup> is 1.5-fold higher in electroautotrophic cells than chemoautotrophic ones (Fig. 2B). Such an increase of redox cofactor pool and a more reduced, electron-rich intracellular status may promote a faster turnover of redox-based metabolic activities (44) and a larger driving force for CO<sub>2</sub> reduction (45).

We also analyzed nucleotides as energy cofactors and found out that abundances of adenosine diphosphate (ADP) and adenosine monophosphate (AMP) are 3-fold higher in electroautotrophic cells than chemoautotrophic cells. Meanwhile, ATP, guanosine diphosphate (GDP), and guanosine monophosphate (GMP) were exclusively detected in electroautotrophic cells (Fig. 2B) possibly owing to their lower abundances in chemoautotrophic conditions, molecule instability and the extended static period required for LC-MS-based metabolomic analysis. Luminescence-based ADP/ATP ratio analysis was conducted and ADP/ATP ratios in electroautotrophic and chemoautotrophic cells are  $7.7 \pm 0.3$  and  $9.3 \pm 0.5$ , respectively. The generally high value of ADP/ATP ratio, a lower state of adenylate energy charge, is consistent to the values observed in acetogenic *Acetobacterium woodii* in chemoautotrophy (46), indicative of scarce ATP generation and the thermodynamic limitation in the generally slow-growing acetogens. Yet the increased pool of nucleotide cofactors and lower ADP/ATP ratio observed in electroautotrophic cells than the chemoautotrophic ones imply a more active cellular metabolism under electricity supply (47).

Moreover, the increased cofactors abundance in H<sub>2</sub>-mediated electroautotrophic *S. ovata* is consistent with the abundance changes of key intermediates in the Wood-Ljungdahl pathway (36). Both electroautotrophic and chemoautotrophic samples exhibit detectable amounts of methenyl-tetrahydrofolate (CH-THF) and methyl-tetrahydrofolate (CH<sub>3</sub>-THF), hence affording

the expression of Wood-Ljungdahl pathway (Fig. 2B, 2C). Yet acetyl coenzyme A (acetyl-CoA), the key intermediate before the generation of ATP and acetic acid via substrate-level phosphorylation, was only detectable in chemoautotrophic cells. The undesired accumulation of acetyl-CoA in chemoautotrophic cells hints that bacterial cells in the materials-biology hybrid are more efficient in converting acetyl-CoA to acetate for ATP production, a limiting factor of Wood-Ljungdahl pathway (36), consistent with the lower ADP/ATP ratio in electroautotrophy than chemoautotrophy ( $7.7 \pm 0.3$  vs.  $9.3 \pm 0.5$ ) and a faster kinetic of ATP production. Those results corroborate a CO<sub>2</sub>-fixing mechanism in electroautotrophy not only more active but also more energy efficient in the context of ATP generation.

There are two more noteworthy metabolomic differences between electroautotrophic and chemoautotrophic cells. First, one of the largest abundance changes of intracellular metabolites is the 150- to 500-fold increase of N-acetyl-amino acids, such as acetyl-glutamate, acetyl-ornithine, and acetyl-lysine, in the electroautotrophic cells (Fig. 2D). The magnitude of such abundance change, in conjunction of their possible implication towards the osmotic protection (48), offers some intriguing clues toward a hypothesized shift of membrane electrochemical potential ( $\Delta\mu_{\text{proton}}$ ) in the materials-biology hybrid (see below). Second, we attempted extracting the extracellular metabolites in both scenarios and searching for additional extracellular redox mediators. Intracellularly, redox-active riboflavin (Fig. 2E), flavin adenine dinucleotide (FAD) and flavin mononucleotide (FMN) (Supplementary Fig. S7) were detected under both electroautotrophic and chemoautotrophic conditions. Yet only riboflavin was also detected extracellularly under both conditions, albeit at a much diluted concentration on the order of nM (Supplementary Table S3). This extracellular concentration of riboflavin is too low to contribute significantly if anything to the delivery of reducing equivalent and CO<sub>2</sub> fixation but may serve as a signal molecule towards an altered microbial metabolism in the H<sub>2</sub>-mediated materials-biology hybrids.

### **Materials induced differential gene expression during electroautotrophic conditions**

1,993 proteins of *S. ovata* were detected in chemoautotrophic and electroautotrophic cultures (detailed annotations and abundances are available in Supplementary Table S4), among the annotated *S. ovata* DSM2662 genome encoding 5,103 proteins (Uniprot Proteome ID: UP000015521) (49). 1,697 proteins were stably expressed (fold change < 1.5) under both conditions (Fig. 3A). Among the five hydrogenases that were annotated in the genome of *S. ovata*

(50), one [NiFe] hydrogenase and two [Fe] hydrogenases were detected with similar level of expression. Such results support H<sub>2</sub> as the primary energy source for microbial CO<sub>2</sub> fixation under both chemoautotrophic and H<sub>2</sub>-mediated electroautotrophic conditions, and that the rate of H<sub>2</sub> delivery should not contribute significantly to the observed difference in e<sup>-</sup> efficiency. All the enzymes involved in the Wood-Ljungdahl pathway including formate dehydrogenase (FdhA), formyl-THF synthase (Fhs), methenyl-THF cyclohydrolase (FchA), methylene-THF dehydrogenase (FolD), Methylene-THF reductase (MetFV), CO dehydrogenase/Acetyl-CoA synthase (AcsABCDEFV & CooC) and acetate kinase (AckA) were all stably expressed in both electroautotrophic and chemoautotrophic cells (Fig. 3B, 3C). The lack of statistically significant changes in abundance indicates that microbial capability of CO<sub>2</sub> fixation into acetic acid remained unperturbed in the materials-biology hybrid. Such result also suggests that other factors connected to but not within the Wood-Ljungdahl pathway, such as ATP generation as one key limiting factor for acetogenic organisms (see above) (51), are potentially responsible for the observed difference in e<sup>-</sup> efficiency (Fig. 1D, 1E).

We also observed significant differences (fold change  $\geq 1.5$  and  $p < 0.05$ ) of gene expressions in some key proteins that hints a favored membrane-based proton translocation and ATP generation in *S. ovata* grown electroautotrophically. Differential gene expression was observed that 102 proteins were up-regulated in *S. ovata* cells grown with electrochemical system while 194 proteins were up-regulated in cells grown under H<sub>2</sub>-containing headspace (Fig. 3A). Notably, the subunit of ATP synthase (AtpH), the enzyme responsible for ATP generation based on proton translocation (52), is up-regulated in the materials-biology hybrid (Fig. 3B). This corroborates an enhanced ATP production under the bioelectrochemical condition as observed in metabolomic analysis. Meanwhile, ferredoxin:NAD<sup>+</sup> oxidoreductase (Rnf) and heterodisulfide reductase subunit C (HdrC), the two enzymes that are reported to sequentially translocate H<sup>+</sup> and generate transmembrane proton gradient by a series of membrane-bound electron transfer (53-55), are either stably expressed for Rnf or up-regulated for HdrC. Such information suggest that the establishment of transmembrane H<sup>+</sup> gradient is favored in the electroautotrophic condition. Such an argument is corroborated by the observed up-regulation of cytochrome *bd* ubiquinol oxidase (Cyt *bd*) subunit A (Cyd A) and several proteins neighboring the same gene cluster (Fig. 3B), which are the putative components of the electron transport chain that connects HdrC via ubiquinol pool (Fig. 3C) (55). Meanwhile, the Na<sup>+</sup>/H<sup>+</sup> antiporter (Nha) involved in maintaining cytosol pH

homeostasis (56) was found significantly up-regulated under electroautotrophic conditions. This observation suggests a shift and possible regulation of  $\Delta\mu_{\text{proton}}$  in electroautotrophic *S. ovata* cells as discussed in-depth below.

### **Integrated omic-analysis unraveled metabolic rewiring**

Our experimental observations collectively support a more active and efficient metabolism in the materials-biology hybrid, for the generation of energy carriers and the reduction of CO<sub>2</sub> into acetic acid. We demonstrated a H<sub>2</sub>-mediated electroautotrophy, based on the absence of noticeable biofilm formation on Co-P alloy cathode (Fig. S5), the estimated percentage of more than 99.9% for planktonic cells, and the inability of detecting other known redox mediators at appreciable concentrations (> nM). We observed an accelerated production of acetic acid and increased values of  $e^-$  efficiency (Fig. 1D, 1E, Supplementary Table S1), even though the hybrid system consumed similar amounts of reducing equivalent namely H<sub>2</sub> as the chemoautotrophic ones do under the similar levels of hydrogenase expression in both conditions. Additional experiments under different methods of H<sub>2</sub> delivery suggest that mass transport of H<sub>2</sub> does not contribute to such observed differences of  $e^-$  efficiency. Instead, it is the significant difference in thermodynamic Gibbs free energies of CO<sub>2</sub> reduction ( $\Delta G$ ) under different H<sub>2</sub> partial pressures that leads to drastic observed difference of chemoautotrophic CO<sub>2</sub>-fixing rates between 1% and 80% H<sub>2</sub> partial pressure.  $\Delta G$  is calculated to be  $-16.7$  and  $-27.8$  kJ/mol per one equivalent of H<sub>2</sub> for 1% and 80% H<sub>2</sub> partial pressures at 1 bar, respectively, under otherwise the same physiological conditions (Supplementary Fig. S8). It is remarkable that the more efficient electroautotrophy (Entry 1 and 2 in Supplementary Table S1) occurs at a much lower H<sub>2</sub> partial pressure, i.e. against a less favored  $\Delta G$ , than the compared chemoautotrophic ones with 80% H<sub>2</sub> at 1 bar in the headspace (Entry 3 and 4 in Supplementary Table S1).

Meanwhile, the abundance of redox-active and more importantly non-redox-based energy cofactors, quantitatively assayed via measuring the NADH/NAD<sup>+</sup> and ADP/ATP ratios, indicated that intracellular conditions in the hybrid system were more reduced and energy-rich (Fig. 2B), while the metabolic activities and protein expressions in the Wood-Ljungdahl pathway remained largely unperturbed (Fig. 2B, 3B). Such an enhanced metabolic energy supply was consistent with the up-regulated expression of ATP synthase and other proteins related to the generation of transmembrane proton gradient (Fig. 3B, 3C). In the Wood-Ljungdahl pathway (36), acetogenic

organisms are quite ATP-limited under chemoautotrophic conditions due to the net zero ATP synthesis by substrate-level phosphorylation. The organisms are predicted to yield at most 0.5 to 1.5 ATP through the transmembrane  $H^+$  gradient for each acetic acid molecule after an 8-electron reduction of  $CO_2$  (57, 58). Hence our observations suggest that the efficiency of ATP generation in *S. ovata* was increased in the materials-biology hybrid.

We hypothesize that the up-regulated expression of Hdr and cytochromes contribute to an increased  $H^+$  translocation hence microbial generation of ATP in electroautotrophic conditions (Fig. 4). *S. ovata* is reported to generate transmembrane proton gradient hence ATP through a confurcation mechanism (55), in which ferredoxin generated by electron-bifurcating hydrogenase (Bif) first transforms to NADH via proton-pumping Rnf and subsequently to  $NAD^+$  via a  $H^+$ -pumping electron transport chain including ubiquinol, Hdr, and speculatively cytochromes (Cyt) (Fig. 4). Our observed up-regulation of Hdr and cytochromes will potentially increase the extent of the second  $H^+$ -pumping step by the confurcation mechanism. Such metabolic shift in the materials-biology hybrid can alleviate the limited ATP yield with faster microbial  $CO_2$  fixation and a higher  $e^-$  efficiency.

A relevant side evidence supporting the proposed increase of proton translocation resides in the observed significant up-regulation of  $Na^+/H^+$  antiporter (Nha) expression and the increased accumulation of N-acetyl-glutamate in the  $H_2$ -mediated materials-biology hybrids (Fig. 4). While there is a sufficient thermodynamic driving force of  $CO_2$  fixation at 80%  $H_2$ , at low  $H_2$  partial pressure as the case of electroautotrophy it is critical to maintain a hemostasis of suitable membrane proton electrochemical potential ( $\Delta\mu_{proton}$ ), typically  $-140$  to  $-200$  mV as commonly reported (56), in order to satisfy two contradicting factors for sustained  $CO_2$  fixation (Supplementary Fig. S9, more detailed discussion in Supplementary Note 2). First, a negative enough  $\Delta\mu_{proton}$  must be maintained in order to have sufficient energy to drive ATP formation owing to the structural  $H^+/ATP$  stoichiometry of ATP synthase (59); second,  $\Delta\mu_{proton}$  cannot be too negative in order to thermodynamically enable  $H^+$ -pumping in aforementioned coupling sites driven by exergonic redox reactions (56). Therefore, ideally a suitable  $\Delta\mu_{proton}$  level tailored to the specific  $H_2$  partial pressure must be maintained to enable  $CO_2$  fixation in acetogens, and a less negative  $\Delta\mu_{proton}$  better suits a lower  $H_2$  partial pressure owing to change of  $\Delta G$  values for  $CO_2$  fixation. As  $Na^+/H^+$  antiporter (Nha) is known to modulate pH homeostasis by exchanging extracellular  $H^+$  with intracellular  $Na^+$  hence increasing the value of  $\Delta\mu_{proton}$  (Supplementary Note

2, Fig. S9), our observed significant up-regulation of Nha during electroautotrophy is consistent with the expected shift of  $\Delta\mu_{\text{proton}}$  for sustained CO<sub>2</sub> fixation under low H<sub>2</sub> partial pressure. Similarly, the accumulation of acetyl-glutamate, a common osmolyte (48), could be explained as a response towards the increased osmotic pressure due to the extensive loss of intracellular Na<sup>+</sup>. The electroautotrophic condition is hypothesized to re-wire the metabolism by modulating  $\Delta\mu_{\text{proton}}$  and achieve a balance between proton-pumping at coupling sites and ATP synthesis, which is not present under chemoautotrophic conditions under similarly low H<sub>2</sub> partial pressure.

At this moment, it remains speculative about how the bacterial cells “sense” the electrochemistry under the seemingly simple H<sub>2</sub>-mediated process. We hypothesize that it is the trace amount of extracellularly redox-active biomolecules such as riboflavin detected in our experiments that putatively signal the metabolic rewiring. The stable expression level of hydrogenase, as well as the slow if any chemoautotrophic CO<sub>2</sub> fixation under similarly low H<sub>2</sub> pressures, preclude H<sub>2</sub> as the signaling pathway in electroautotrophy. Therefore, other signaling pathways, probably redox-based, must be present in addition to the H<sub>2</sub>-mediated materials-biology hybrids. We detected intracellular FAD, FMN and riboflavin in all tested conditions (Fig. 2E, Supplementary Fig. S7). Small amount of extracellular riboflavin was also detected at most on the order of nM (Supplementary Table S3), which is too low to contribute significant delivery of reducing equivalents for CO<sub>2</sub> fixation. Yet soluble redox-active electron shuttles, commonly derivatives of flavins, quinones, and cytochromes, are known to mediate long-distance electron transfer at a redox potential close to HER (60, 61) and trigger metabolic rewiring in microorganisms (62). Such literature precedence leads us to speculate that the extracellular riboflavin (−210 mV vs. SHE) (63) might serve as a redox-sensing signal molecule, previously underappreciated in the *S. ovata* system, and trigger the observed metabolic rewiring including a tailored  $\Delta\mu_{\text{proton}}$  level, up-regulated Hdr and Cyt for proton translocation, more efficient ATP generation, and a more reduced intracellular redox state for H<sub>2</sub>-mediated microbial CO<sub>2</sub> fixation (Fig. 4).

## Discussion

In this work, we showcase the previously undetected metabolic rewiring in *S. ovata* from a H<sub>2</sub>-mediated materials-biology hybrid. Such results illustrate the metabolic versatility and complexity of *S. ovata*, thanks to its high *e*<sup>−</sup> efficiency of CO<sub>2</sub> fixation (64), robustness towards

extragenic interferences (65), and the plentiful redox-based coupling sites involving ubiquinol and cytochromes (54). Future studies about the detailed signaling pathway between the microbes and the water-splitting electrodes will be welcomed and should yield useful insights about proton translocation and ATP generation that are critical in the CO<sub>2</sub>-fixing Wood-Ljungdahl pathway. Such insights will be beneficial for the design of hybrid systems for sustainable CO<sub>2</sub> fixation with *S. ovata* as the biotic component.

Moreover, our unexpected observation of the fortuitous metabolic rewiring highlights the necessity of thorough examination about the interactions in materials-biology hybrids. We posit that the observed metabolic rewiring may exist in a wide range of seemingly simple H<sub>2</sub>-mediated hybrid systems with potential benefits that so far have been under-appreciated and under-utilized. In addition to the extensive research efforts being devoted towards materials design and synthetic biology for the efficient production of targeted chemicals in the hybrids (1, 2, 4), we advocate the deployment of multi-omic studies for a comprehensive understanding of microbial metabolism in search of unexpected synergies. Such research efforts will enable us to maximize the efficiency and throughput of CO<sub>2</sub> fixation using the materials-biology hybrids for a sustainable future.

## Materials and Methods

### Materials and chemicals

The chemicals and materials were purchased from Sigma-Aldrich (St. Louis, MO, USA), unless otherwise specified. The carbon cloth was purchased from Fuel Cell Earth (Woburn, MA, USA) and the stainless-steel mesh was purchased from Alfa Aesar (Ward Hill, MA, USA). The  $^1\text{H}$  NMR standard sodium 3-(trimethylsilyl) propionate 2,2,3,3-D<sub>4</sub> (TSP-D<sub>4</sub>) and deuterium oxide (purity > 99.9%) were obtained from Cambridge Isotope Laboratories, Inc (Tewksbury, MA, USA). Methanol, acetonitrile, ammonium acetate, ammonium hydroxide, and acetic acid were purchased from Fisher Scientific (Waltham, NJ, USA).

### Electrode fabrication and characterization

The cathode and anode were coated with Co-P alloy and cobalt phosphate (CoPi) catalysts, respectively, using electrochemical deposition following established protocols (7, 14, 31). A single-chamber electrochemical setup installed with a working electrode of deposition substrate, a Pt counter electrode, and a Ag/AgCl (1M KCl) (CH Instrument, Austin, TX, USA) reference electrode, was connected to Gamry Interface 1000 potentiostat (Gamry Instruments, Warminster, PA, USA). The Co-P alloy cathode was prepared by a 15-min chronoamperometry in an electrolyte consisted of 0.15 M  $\text{H}_3\text{BO}_3$ , 0.1 M NaCl, 0.33 M  $\text{NaH}_2\text{PO}_2\cdot\text{H}_2\text{O}$  (sodium hypophosphite), and 0.2 M  $\text{CoCl}_2\cdot 6\text{H}_2\text{O}$ , during which the stainless-steel mesh was poised at  $-1.5$  V vs. reference electrode. The CoPi anode was deposited on the carbon cloth in an electrolyte consisted of 10 mM  $\text{Co}(\text{NO}_3)_2$  and 0.1 M methylphosphonate with a pH adjustment to 8. Chronocoulometry was performed with an applied potential of 0.85 V vs. reference electrode until  $500 \text{ mC cm}^{-2}$  of charge was transferred.

The morphologies and element compositions of electrocatalysts (Supplementary Fig. S2) were characterized by JEOL JSM-6700F field emission scanning electron microscope (JOEL, Peabody, MA, USA) equipped with Ametek energy dispersive X-ray spectroscopy (EDS) (EDAX-AMETEK, Mahwah, NJ, USA), or ZEISS Supra 40VP field emission scanning electron microscope (ZEISS, Oberkochen, Germany), after Au sputtering with Hummer 6.2 sputter coater (Anatech, Sparks, NV, USA). A pretreatment followed an established protocol (33) was applied for the electron-microscopy characterization of Co-P cathode with potentially adhered cells. The cathode was fixed in 2.5% glutaraldehyde overnight and sequentially immersed in ethanol (25%,



50%, 75%, 90%, 100%, 10 min each), and then transferred into hexamethyldisilazane (HMDS) for 1 hour (hr). The cathode was left to air dry overnight prior to characterization.

### **Chemoautotrophic culturing of *Sporomusa ovata***

The *S. ovata* were routinely maintained at 30 °C in 160 mL serum bottles containing 100 mL of mineral salts medium (66, 67) (Supplementary Note 1) closed with butyl rubber stoppers (Chemglass Life Sciences LLC, Vineland, NJ, USA) held in place with aluminum crimps. The headspace was filled with 1-bar H<sub>2</sub>:CO<sub>2</sub> (80:20, v:v) with sufficient agitation. For the growth comparison under different conditions, the inoculum of H<sub>2</sub>-grown *S. ovata* cells were transferred in biological triplicates.

The chemoautotrophic cultures were grown at 30 °C in the 160-mL serum bottle containing 50 mL mineral salts medium (Supplementary Note 1), 50 mL inoculum and 60 mL headspace, which were maintained under similar if not the same experimental conditions as the electroautotrophic cultures except for the electron donor (see below). H<sub>2</sub> was intermittently supplied to the chemoautotrophic cultures by replacing the headspace (60 mL) with H<sub>2</sub>:CO<sub>2</sub> (80:20, v:v) every 12 hr at 1 bar with sufficient agitation. Under such conditions, *S. ovata* utilized H<sub>2</sub> as the sole electron donor and CO<sub>2</sub> and NaHCO<sub>3</sub> as the carbon sources. All cultures were grown under strictly anoxic conditions in the presence of reducing reagents of 0.2 mM Na<sub>2</sub>S and 0.2 mM cysteine. At least two independent batch experiments, each with three replicates, were performed for the sake of reproducibility (Entry 3 and 4 in Supplementary Table S1). A negative control was performed on the same medium for *S. ovata* growth in the absence of electricity or H<sub>2</sub> and the headspace was replaced by N<sub>2</sub>:CO<sub>2</sub> (80:20, v:v) every 12 hr at 1 bar (Supplementary Fig. S3). Chemoautotrophic growth of *S. ovata* was also tested in the same bioelectrochemical setup meant for electroautotrophic growth (see below) yet in the absence of electricity. Instead, a continuous gas flow of H<sub>2</sub>:CO<sub>2</sub>:N<sub>2</sub> (1:20:79, v:v:v) was bubbled to the setup, mimicking if not replicating the mass transport and the delivery of H<sub>2</sub> in electroautotrophy, under similar experimental conditions as the electroautotrophic cultures except for the electron donor. Two different gas flow rates of 6 mL min<sup>-1</sup> and 4 mL min<sup>-1</sup>, controlled by the mass flow controller (Omega Engineering, Norwalk, CT, USA), were tested with almost the same results (Entry 5 and 6 in Supplementary Table S1). Aliquot samples were taken from the cathodic chamber periodically for further analysis.

## Electroautotrophic materials-biology hybrids of *Sporomusa ovata*

The electroautotrophic cultures were established with triplicates following previously reported procedure with slight modifications (31). Customized three-electrode, two-chamber (150 mL each) electrochemical cells (H cells), separated by Nafion 117 membrane (Chemours, Wilmington, DE, USA), were applied for *S. ovata* incubation to allow the proton exchange (Supplementary Fig. S1). The gas-tight cathodic chamber had been flushed with N<sub>2</sub>:CO<sub>2</sub> (80:20, v:v) to maintain the anoxic environment, followed by the transfer of the mineral salts medium (50 mL) and *S. ovata* inoculum (50 mL) under strict anoxic conditions. The cathode chamber includes Co-P cathode and leak-free Ag/AgCl reference electrode (+0.209 V vs. standard hydrogen potential, SHE, Innovative Instruments, Inc., Tampa, FL, USA) under a constant gas supply of N<sub>2</sub>:CO<sub>2</sub> (80:20, v:v) at the rate of 6 mL min<sup>-1</sup> controlled by the mass flow controller. In order to maintain similar if not the same gas transport as the case of chemoautotrophic growth (see above), the gas supply is purged over the headspace of cathodic chamber. The anodic chamber includes CoPi anode and the headspace was continuously flushed with N<sub>2</sub>:CO<sub>2</sub> (80:20, v:v). Both chambers were stirred at the constant rate of 150 rpm and placed in a water bath maintained at 30 °C during the three-day experiment. Aliquot samples were taken from the cathodic chamber periodically for further analysis.

The electrochemical settings of electroautotrophic cultures were achieved with a Gamry Interface 1000E potentiostat interfaced with a Gamry 8-channel ECMB multiplexer. The electrochemical potentials ( $E$ ) have been  $iR$  compensated with the solution series resistance determined daily by electrochemical impedance spectroscopy, and are all referenced to SHE using the following equation (1):

$$E_{\text{vs. SHE}} = E_{\text{vs. Ag/AgCl}} + 0.209 \text{ V} \quad (1)$$

Cyclic voltammetry between  $-0.39 \text{ V}$  to  $-1.39 \text{ V}$  vs. SHE at a scan rate of  $50 \text{ mV s}^{-1}$  was conducted daily to check the system's stability. Multiplexed chronoamperometry, whose  $E$  values are adjusted daily to maintain a desired level of current intensity, was performed to ensure electroautotrophic systems.

## Residual extracellular oxidizable organics carried over during bacterial inoculation

The chemical oxygen demand (COD) in the extracellular components of the culture after *S. ovata* inoculation was analyzed in order to more accurately quantify the  $e^-$  efficiency of CO<sub>2</sub>

fixation. The extracellular components were collected by filtering culture through sterile polyethersulfone membrane (0.22  $\mu\text{m}$ , Avantor, Radnor, PA, USA) to exclude planktonic *S. ovata* cells. Colorimetric COD analysis was performed using TNT82206 kit (Hach, Loveland, CO, USA.) following the manufacturer's protocol, after establishing a standard curve prepared in the same mineral salts medium to avoid any matrix effects interfering with the quantification. The potential electron storage in the extracellular oxidizable component in carryover was calculated based on the equation (2).

$$N_{e,\text{carryover}} \text{ (mmole)} = \text{COD (mmole)} \times 4 - N_{\text{acetate}} \text{ (mmole)} \times 8 \quad (2)$$

Here COD represents the amount of oxygen required to completely oxidize the extracellular components,  $N_{\text{acetate}}$  the observed generation of extracellular acetate (see below), and  $N_{e,\text{carryover}}$  presents the amount of reducing equivalents, in the unit of millimoles (mmole) of electrons, that can contribute to bacterial  $\text{CO}_2$  fixation. Here we assume that 1 COD equivalent offers 4 electron equivalents and the formation of one equivalent acetate requires 8 electron equivalents via  $\text{CO}_2$  fixation.

### Product quantification and electron efficiency analysis

The liquid products in the sampled aliquots were quantified by the 400 MHz Nuclear Magnetic Resonance (NMR) spectrometer (Bruker, Billerica, MA, USA) equipped with Bruker AV400 Sample Changer. The acetate concentration was quantified using the chemical shift of 1.92 ppm in  $^1\text{H}$  NMR spectroscopy on a liquid sample containing culture suspension and internal standard of TSP-D4 (31), after the establishment of a standard calibration curve. The total amount of acetate accumulation was calculated based on the measured acetate concentration and liquid volume. The  $\text{H}_2$  partial pressure in the culture headspace was measured by an 8610C gas chromatography system (SRI Instruments, Torrance, CA, USA) equipped with Hayesep D and MS 5A packed columns, and a thermal conductivity detector (TCD) (16). The total amount of  $\text{H}_2$  in the liquid culture was calculate every 12 hours based on measured  $\text{H}_2$  partial pressure, by considering both the gaseous and dissolved  $\text{H}_2$  with additional inputs of the monitored headspace gas pressure (McMaster-Carr, Elmhurst, IL, USA) and the known  $\text{H}_2$  solubility with a Henry solubility coefficient of  $7.7 \times 10^{-6} \text{ mole m}^{-3} \text{ Pa}^{-1}$  (68). Last, the protein concentrations in *S. ovata* cultures were determined using the Bradford assay following an established protocol (42). Lysed culture suspension was prepared by treating 0.5-mL culture suspension in a boiling water bath,

then mixed with Pierce Coomassie reagent (Pierce Coomassie Protein Assay Kit, Thermo Scientific) for a colorimetric analysis of 595-nm absorbance using Cary 60 UV-Vis spectrophotometer (Agilent Technologies, Santa Clara, CA, USA), following the manufacturer's protocol after establishing a calibration curve with albumin as the standard sample.

The apparent electron efficiencies ( $e^-$  efficiencies)  $\eta_{app}$  under electroautotrophic and chemoautotrophic conditions ( $\eta_{app,electro}$  and  $\eta_{app,chemo}$ , respectively), without considering potential contribution from the extracellular organics carried over from inoculation, were calculated using the equations (3) and (4), respectively.

$$\eta_{app,electro} = \frac{\Delta C_{acetate} \times V_{medium} \times 8}{\int_{t_0}^t Idt \times F} \times 100\% \quad (3)$$

$$\eta_{app,chemo} = \frac{\Delta C_{acetate} \times V_{medium} \times 8}{\Delta N_{H_2} \times 2} \times 100\% \quad (4)$$

Here  $\Delta C_{acetate}$  represents concentration change of acetate that each requires 8 electrons from  $CO_2$  reduction,  $V_{medium}$  the total volume of liquid culture,  $\int_{t_0}^t Idt$  the total amount of charge transfer during electroautotrophy,  $F$  the Faraday constant ( $96,485 \text{ C mole}^{-1}$ ), and  $\Delta N_{H_2}$  the amount of  $H_2$  consumed during chemoautotrophy that each contributes two electrons for  $CO_2$  reduction.

Moreover, because we found that the extracellular organics carried over from bacterial inoculation contribute appreciable amount of reducing equivalents towards bacterial metabolism (see above), it is more appropriate to calculate the corrected  $e^-$  efficiencies  $\eta$  by accounting the reducing equivalents in extracellular organics ( $N_{e,carryover}$ ) for both electroautotrophic ( $\eta_{electro}$ ) and chemoautotrophic ( $\eta_{chemo}$ ) conditions, respectively:

$$\eta_{electro} = \frac{\Delta C_{acetate} \times V_{medium} \times 8}{\int_{t_0}^t Idt \times F + N_{e,carryover}} \times 100\% \quad (5)$$

$$\eta_{chemo} = \frac{\Delta C_{acetate} \times V_{medium} \times 8}{\Delta N_{H_2} \times 2 + N_{e,carryover}} \times 100\% \quad (6)$$

Both apparent and corrected  $e^-$  efficiencies under each experimental condition were reported in Supplementary Table S1.

### Luminescence-based ADP/ATP ratio analysis

The two-step D-luciferin based ADP/ATP ratio analysis was performed using MAK15 kit (Sigma-Aldrich) following the manufacturer's protocol. 10- $\mu$ L bacterial culture under both electroautotrophic and chemoautotrophic conditions were collected immediately after the three-day experiments and instantly mixed with reaction reagent on a 96-well plate with a clear bottom.

The luminescence intensities were recorded by microplate reader SpectraMax iD3 (Molecular Devices, San Jose, CA, USA) and the ADP/ATP ratio was calculated following manufacture's protocol.

### **Metabolome extraction and sample preparation**

After a three-day experiment, 1-mL bacterial suspension was vacuum-filtered on a nylon membrane (25 mm diameter, 0.2  $\mu\text{m}$  pore size, Millipore, Burlington, MA, USA). The membrane was immediately transferred to a 6-well plate containing 1 mL of cold extraction solvent for non-folate species ( $-20^{\circ}\text{C}$ , 40:40:20, methanol/acetonitrile/water) to quench metabolism. For intracellular folate species, the extraction solvent was 80:20 acetonitrile/water with 2.5 mM sodium ascorbate and 25 mM ammonium acetate stored at  $4^{\circ}\text{C}$  for stability. After 20 min of metabolite extraction at the respective cold temperatures, the cell extract was collected, transferred to a microcentrifuge tube, and centrifuged at  $17,000 \times g$  for 10 min at  $4^{\circ}\text{C}$ . The supernatant was transferred to a new centrifuge tube, dried under nitrogen flow, and reconstituted in LC-MS (liquid chromatography-mass spectrometry) grade water before transferring to vials for LC-MS analysis (69). Additionally, to determine extracellular metabolites, the filtrate of bacterial suspension was diluted with LC-MS grade methanol at a 20:80 ratio. After centrifuging at  $17,000 \times g$  for 10 min at  $4^{\circ}\text{C}$ , supernatants were transferred to vials for later LC-MS analysis.

### **Metabolomics analysis**

LC separation was achieved in a Vanquish UHPLC system (Thermo Fisher Scientific, Bremen, Germany) equipped with a hydrophilic interaction chromatography column (Xbridge BEH Amide XP column,  $130\text{\AA}$ ,  $2.5 \mu\text{m}$ ,  $2.1 \text{ mm} \times 150 \text{ mm}$ , Waters, Milford, MA). Mobile phases were 20 mM ammonium acetate and 20 mM ammonium hydroxide in 95:5 water:acetonitrile (pH 9.4) as eluent A and acetonitrile as eluent B. Column temperature set at  $25^{\circ}\text{C}$ , and a flow rate was  $150 \mu\text{L min}^{-1}$ . The gradient was as follows: 90% B at 0 min, 90% B at 0.5 min, 75% B at 1.5 min, 75% B at 5.5 min, 70% B at 6.5 min, 70% B at 7.5 min, 50% B at 8.5 min, 50% B at 10.5 min, 25% B at 11.5 min, 25% B at 12.5 min, 0% B at 14.5 min, 0% B at 20 min, 90% B at 20.5 min, 90% B at 26 min. The total run time was 26 min at a flow rate of  $150 \mu\text{L min}^{-1}$  (70). The injection volumes were 2 and  $10 \mu\text{L}$  for extracellular and intracellular metabolite samples, respectively. LC separation of folates species was on a reversed-phase column (Agilent InfinityLab Poroshell 120

Bonus-RP 2.7  $\mu\text{m}$ , 2.1  $\times$  150 mm) with 10 mM ammonium acetate and 0.1% vol of acetic acid in 95:5 water:acetonitrile as eluent A and acetonitrile as eluent B. Gradient conditions were 2% B at 0 min, 98% B at 20 min, 98% B at 25min, 2% B at 26 min, 2% at 35 min. The flow rate was 200  $\mu\text{L min}^{-1}$ , and the column temperature was 25  $^{\circ}\text{C}$ . The injection volume was 20  $\mu\text{L}$ .

For mass spectrometry, the above-described LC systems were interfaced with Q-Exactive Plus Hybrid Quadrupole-Orbitrap Mass Spectrometer (Thermo Fisher Scientific). The mass spectra were collected in positive mode scanning mass-to-charge ( $m/z$ ) ratio range between 60 to 900, and negative mode scanning  $m/z$  60 to 200 and  $m/z$  200 to 2,000 at a resolution of 140,000 at  $m/z$  200, with automatic gain control (AGC) target 3e6, and maximum injection time (IT) of 500 ms. For folate species, mass spectra were collected only in positive scanning  $m/z$  442 to 476 at a resolution of 35,000 at  $m/z$  200, and a maximum IT of 200 ms. The authenticated standards including more than 400 metabolites were applied to verify the retention time (71). For MS/MS analysis, full MS/dd-MS2 mode was used. Full MS was in positive scanning  $m/z$  100 to 1000 at a resolution of 140,000 at  $m/z$  200, and a maximum IT of 120 ms. MS/MS scanning was with a resolution of 70,000 at  $m/z$  200, a maximum IT of 100 ms, an isolation window of 2  $m/z$ , minimum AGC 1.0e3, and normalized collision energy (NCE) of 30 with an inclusion list of targeted metabolites.

Data were collected using Thermo Scientific Xcalibur data acquisition and interpretation software (version 4.2.27) and Q-Exactive MS series Tune interface (version 2.11). Data analysis was processed using the Maven software package (72). Metabolite identification was based on the exact  $m/z$  with mass error less than 10 ppm and a retention time difference smaller than 1 min to the authenticated standards (70). The abundance of each metabolite was reported after integrating the top peak area in extracted ion chromatogram and normalized to the protein concentration in culture.

### **Proteome extraction and sample preparation**

After a three-day experiment, cell pellets from 40 mL culture suspensions were collected by centrifuging at 7,547  $\times$  g for 20 minutes using Sorvall ST 8 centrifuge (Thermo Fisher Scientific). The proteome was extracted using the established protocol (16). Cell pellets were resuspended in 0.5-mL lysis buffer consisted of 100 mM Tris, 8 M urea, 35 mM sodium dodecyl sulfate, protease inhibitor (Thermo Fisher Scientific), and benzonase nuclease (MilliporeSigma,

Burlington, MA, USA), and sonicated using the point sonicator for 10 seconds on the ice bath followed by rotation at 4°C for 30 minutes. The proteins present in the supernatant were collected by centrifuging at 16,000 × g for 15 minutes at 4°C. The proteins were reduced, alkylated and digested following the established procedures (16). Following the digestion, the peptides eluted from carboxylate-modified magnetic beads were dried by vacuum centrifugation and reconstituted in 5% formic acid before analysis by LC-MS/MS (Liquid chromatography - tandem mass spectrometry).

### **Proteomics analysis**

Peptide samples were separated on a 75 µm ID, 25 cm C18 column packed with 1.9 µm C18 particles (Dr. Maisch GmbH HPLC, Ammerbuch, Germany) using a 140-minute gradient of increasing acetonitrile concentration and injected into a Thermo Orbitrap-Fusion Lumos Tribrid mass spectrometer. MS/MS spectra were acquired using Data Dependent Acquisition (DDA) mode.

MS/MS database searching was performed using MaxQuant (1.6.10.43) against the *S. ovata* DSM 2662 reference proteome from Uniprot (UP000015521, 5045 entries). The domain annotation and functional prediction of proteins were obtained from UniParc. The KEGG orthology (KO) assignment based on the amino acid sequence of the protein was performed using BlastKOALA which was used for pathway analysis against KEGG database (73).

Statistical analysis of MaxQuant label-free quantitation data was performed with the artMS Bioconductor package which performs the relative quantification of protein abundance using the MSstats Bioconductor package (default parameters). Intensities were normalized across samples by median-centering the log<sub>2</sub>-transformed MS1 intensity distributions. The abundance of proteins missing from one condition but found in more than 2 biological replicates of the other condition for any given comparison were estimated by imputing intensity values from the lowest observed MS1-intensity across samples.

### **Data availability**

The metabolomic and proteomic data reported in this study are available in the Supplementary Data files. Other data that support the plots within this paper and other findings of this study are available from the corresponding author upon reasonable request.

## **Acknowledgements**

C.L. acknowledges the support from National Institute of Health (R35GM138241), Sloan Research Fellowship from Alfred P. Sloan Foundation, and the Jeffery and Helo Zink Endowed Professional Development Term Chair.

## **Additional information**

**Supplementary information** is available in one Word document that includes supplementary information text, supplementary Table S1 to S2, and supplementary Figure S1 to S9. One supplementary data file includes the data for Table S3 to S4.

**Correspondence and requests for materials** should be addressed to Chong Liu.



## References

1. H. Chen, F. Dong, S. D. Minter, The progress and outlook of bioelectrocatalysis for the production of chemicals, fuels and materials. *Nat. Catal.* **3**, 225-244 (2020).
2. D. K. Dogutan, D. G. Nocera, Artificial photosynthesis at efficiencies greatly exceeding that of natural photosynthesis. *Acc. Chem. Res.* **52**, 3143-3148 (2019).
3. N. Kornienko, J. Z. Zhang, K. K. Sakimoto, P. Yang, E. Reisner, Interfacing nature's catalytic machinery with synthetic materials for semi-artificial photosynthesis. *Nat. Nanotechnol.* **13**, 890-899 (2018).
4. O. Adesina, I. A. Anzai, J. L. Avalos, B. Barstow, Embracing biological solutions to the sustainable energy challenge. *Chem* **2**, 20-51 (2017).
5. T. Zhang, More efficient together. *Science* **350**, 738-739 (2015).
6. K. P. Nevin, T. L. Woodard, A. E. Franks, Z. M. Summers, D. R. Lovley, Microbial electrosynthesis: feeding microbes electricity to convert carbon dioxide and water to multicarbon extracellular organic compounds. *mBio* **1**, e00103-00110 (2010).
7. C. Liu, B. C. Colón, M. Ziesack, P. A. Silver, D. G. Nocera, Water splitting–biosynthetic system with CO<sub>2</sub> reduction efficiencies exceeding photosynthesis. *Science* **352**, 1210-1213 (2016).
8. R. S. Sherbo, P. A. Silver, D. G. Nocera, Riboflavin synthesis from gaseous nitrogen and carbon dioxide by a hybrid inorganic-biological system. *Proc. Natl. Acad. Sci. U.S.A.* **119**, e2210538119 (2022).
9. H. Li *et al.*, Integrated electromicrobial conversion of CO<sub>2</sub> to higher alcohols. *Science* **335**, 1596-1596 (2012).
10. B. E. Logan, R. Rossi, A. Ragab, P. E. Saikaly, Electroactive microorganisms in bioelectrochemical systems. *Nat. Rev. Microbiol.* **17**, 307-319 (2019).
11. B. E. Logan, K. Rabaey, Conversion of wastes into bioelectricity and chemicals by using microbial electrochemical technologies. *Science* **337**, 686-690 (2012).
12. K. Rabaey, R. A. Rozendal, Microbial electrosynthesis-revisiting the electrical route for microbial production. *Nat. Rev. Microbiol.* **8**, 706-716 (2010).
13. H. Chen *et al.*, Fundamentals, applications, and future directions of bioelectrocatalysis. *Chem. Rev.* **120**, 12903-12993 (2020).
14. C. Liu, K. K. Sakimoto, B. C. Colón, P. A. Silver, D. G. Nocera, Ambient nitrogen reduction cycle using a hybrid inorganic–biological system. *Proc. Natl. Acad. Sci. U.S.A.* **114**, 6450-6455 (2017).
15. C. Liu *et al.*, Nanowire–bacteria hybrids for unassisted solar carbon dioxide fixation to value-added chemicals. *Nano Lett.* **15**, 3634-3639 (2015).
16. X. Guan *et al.*, Maximizing light-driven CO<sub>2</sub> and N<sub>2</sub> fixation efficiency in quantum dot–bacteria hybrids. *Nat. Catal.* **5**, 1019-1029 (2022).
17. K. K. Sakimoto, A. B. Wong, P. Yang, Self-photosensitization of nonphotosynthetic bacteria for solar-to-chemical production. *Science* **351**, 74-77 (2016).
18. Y. He *et al.*, Photosynthesis of acetate by *Sporomusa ovata*–CdS biohybrid system. *ACS Applied Materials & Interfaces* **14**, 23364–23374 (2022).
19. J. Ye *et al.*, Solar-driven methanogenesis with ultrahigh selectivity by turning down H<sub>2</sub> production at biotic-abiotic interface. *Nat. Commun.* **13**, 6612 (2022).
20. K. Kuruvinashetti, N. Kornienko, Pushing the methodological envelope in understanding the photo/electrosynthetic materials-microorganism interface. *Isience* **24**, 103049 (2021).

21. P. Li, S. Kim, B. Tian, Nanoenabled trainable systems: From biointerfaces to biomimetics. *ACS nano* **16**, 19651-19664 (2022).
22. X. Meng, L. Liu, X. Chen, Bacterial photosynthesis: state-of-the-art in light-driven carbon fixation in engineered bacteria. *Curr. Opin. Microbiol.* **69**, 102174 (2022).
23. J. S. Deutzmann, F. Kracke, W. Gu, A. M. Spormann, Microbial electrosynthesis of acetate powered by intermittent electricity. *Environ. Sci. Technol.* **56**, 16073-16081 (2022).
24. S. A. Patil *et al.*, Selective enrichment establishes a stable performing community for microbial electrosynthesis of acetate from CO<sub>2</sub>. *Environ. Sci. Technol.* **49**, 8833-8843 (2015).
25. T. Krieg, A. Sydow, S. Faust, I. Huth, D. Holtmann, CO<sub>2</sub> to terpenes: autotrophic and electroautotrophic  $\alpha$ -humulene production with *Cupriavidus necator*. *Angew. Chem. Int. Ed.* **57**, 1879-1882 (2018).
26. J. P. Torella *et al.*, Efficient solar-to-fuels production from a hybrid microbial-water-splitting catalyst system. *Proc. Natl. Acad. Sci. U.S.A.* **112**, 2337-2342 (2015).
27. S. Lu, X. Guan, C. Liu, Electricity-powered artificial root nodule. *Nat. Commun.* **11**, 1505 (2020).
28. E. M. Nichols *et al.*, Hybrid bioinorganic approach to solar-to-chemical conversion. *Proc. Natl. Acad. Sci. U.S.A.* **112**, 11461-11466 (2015).
29. A. R. Rowe *et al.*, Methane-linked mechanisms of electron uptake from cathodes by *Methanosarcina barkeri*. *mBio* **10**, e02448-02418 (2019).
30. J. Kim, S. Cestellos-Blanco, Y. Shen, R. Cai, P. Yang, Enhancing biohybrid CO<sub>2</sub> to multicarbon reduction via adapted whole-cell catalysts. *Nano Lett.* **22**, 5503-5509 (2022).
31. R. M. Rodrigues *et al.*, Perfluorocarbon nanoemulsion promotes the delivery of reducing equivalents for electricity-driven microbial CO<sub>2</sub> reduction. *Nat. Catal.* **2**, 407-414 (2019).
32. N. Aryal, P. L. Tremblay, D. M. Lizak, T. Zhang, Performance of different *Sporomusa* species for the microbial electrosynthesis of acetate from carbon dioxide. *Bioresour. Technol.* **233**, 184-190 (2017).
33. S. Cestellos-Blanco *et al.*, Photosynthetic biohybrid coculture for tandem and tunable CO<sub>2</sub> and N<sub>2</sub> fixation. *Proc. Natl. Acad. Sci. U.S.A.* **119**, e2122364119 (2022).
34. Y. Su *et al.*, Close-packed nanowire-bacteria hybrids for efficient solar-driven CO<sub>2</sub> fixation. *Joule* **4**, 800-811 (2020).
35. R. Zhang *et al.*, Proteomic and metabolic elucidation of solar-powered biomanufacturing by bio-abiotic hybrid system. *Chem* **6**, 234-249 (2020).
36. S. W. Ragsdale, E. Pierce, Acetogenesis and the Wood-Ljungdahl pathway of CO<sub>2</sub> fixation. *Biochim. Biophys. Acta* **1784**, 1873-1898 (2008).
37. N. Aryal *et al.*, Increased carbon dioxide reduction to acetate in a microbial electrosynthesis reactor with a reduced graphene oxide-coated copper foam composite cathode. *Bioelectrochemistry* **128**, 83-93 (2019).
38. N. Jiang, B. You, M. Sheng, Y. Sun, Electrodeposited cobalt-phosphorous-derived films as competent bifunctional catalysts for overall water splitting. *Angew. Chem.* **127**, 6349-6352 (2015).
39. B. Möller, R. Oßmer, B. H. Howard, G. Gottschalk, H. Hippe, *Sporomusa*, a new genus of gram-negative anaerobic bacteria including *Sporomusa sphaeroides* spec. nov. and *Sporomusa ovata* spec. nov. *Arch. Microbiol.* **139**, 388-396 (1984).

40. N. Uría, X. Muñoz Berbel, O. Sánchez, F. X. Muñoz, J. Mas, Transient storage of electrical charge in biofilms of *Shewanella oneidensis* MR-1 growing in a microbial fuel cell. *Environ. Sci. Technol.* **45**, 10250-10256 (2011).
41. M. Y. El-Naggar *et al.*, Electrical transport along bacterial nanowires from *Shewanella oneidensis* MR-1. *Proc. Natl. Acad. Sci. U.S.A.* **107**, 18127-18131 (2010).
42. Y. Xie *et al.*, *Pseudomonas* sp. strain 273 degrades fluorinated alkanes. *Environ. Sci. Technol.* **54**, 14994-15003 (2020).
43. D. E. Canfield, E. Kristensen, B. Thamdrup, "Thermodynamics and microbial metabolism" in *Adv. Mar. Biol.* (Elsevier, 2005), vol. 48, chap. 3, pp. 65-94.
44. A. Grimalt-Aleman, C. Etlar, K. Asimakopoulos, I. V. Skiadas, H. N. Gavala, ORP control for boosting ethanol productivity in gas fermentation systems and dynamics of redox cofactor NADH/NAD<sup>+</sup> under oxidative stress. *J. CO<sub>2</sub> Util.* **50**, 101589 (2021).
45. S. J. Berrios-Rivera, G. N. Bennett, K. San, The effect of increasing NADH availability on the redistribution of metabolic fluxes in *Escherichia coli* chemostat cultures. *Metab. Eng.* **4**, 230-237 (2002).
46. S. Spahn, K. Brandt, V. Müller, A low phosphorylation potential in the acetogen *Acetobacterium woodii* reflects its lifestyle at the thermodynamic edge of life. *Arch. Microbiol.* **197**, 745-751 (2015).
47. M. H. Buckstein, J. He, H. Rubin, Characterization of nucleotide pools as a function of physiological state in *Escherichia coli*. *J. Bacteriol.* **190**, 718-726 (2008).
48. K. R. Sowers, R. P. Gunsalus, Halotolerance in *Methanosarcina* spp.: role of N-acetyllysine, glutamate, glycine betaine, and K<sup>+</sup> as compatible solutes for osmotic adaptation. *Appl. Environ. Microbiol.* **61**, 4382-4388 (1995).
49. A. Poehlein, G. Gottschalk, R. Daniel, First insights into the genome of the Gram-negative, endospore-forming organism *Sporomusa ovata* strain H1 DSM 2662. *Genome Announc.* **1**, e00734-00713 (2013).
50. J. Madjarov, R. Soares, C. M. Paquete, R. O. Louro, *Sporomusa ovata* as catalyst for bioelectrochemical carbon dioxide reduction: A review across disciplines from microbiology to process engineering. *Front. Microbiol.* **13**, 913311 (2022).
51. N. Chu *et al.*, Microbial electrosynthesis for producing medium chain fatty acids. *Engineering*, 141-153 (2021).
52. D. Litty, V. Müller, ATP synthesis in an ancient ATP synthase at low driving forces. *Proc. Natl. Acad. Sci. U.S.A.* **119**, e2201921119 (2022).
53. P. L. Tremblay, T. Zhang, S. A. Dar, C. Leang, D. R. Lovley, The Rnf complex of *Clostridium ljungdahlii* is a proton-translocating ferredoxin: NAD<sup>+</sup> oxidoreductase essential for autotrophic growth. *mBio* **4**, e00406-00412 (2013).
54. F. P. Rosenbaum, V. Müller, Energy conservation under extreme energy limitation: the role of cytochromes and quinones in acetogenic bacteria. *Extremophiles* **25**, 413-424 (2021).
55. F. Kremp, J. Roth, V. Müller, A third way of energy conservation in acetogenic bacteria. *Microbiol. Spectr.*, e01385-01322 (2022).
56. D. White, J. T. Drummond, C. Fuqua, "Membrane Bioenergetics: The Proton Potential" in *The Physiology and Biochemistry of Prokaryotes*. (Oxford University Press, 2012), chap. 4, pp. 111-141.

57. A. G. Fast, E. T. Papoutsakis, Stoichiometric and energetic analyses of non-photosynthetic CO<sub>2</sub>-fixation pathways to support synthetic biology strategies for production of fuels and chemicals. *Curr. Opin. Chem. Eng.* **1**, 380-395 (2012).
58. K. Schuchmann, V. Müller, Autotrophy at the thermodynamic limit of life: a model for energy conservation in acetogenic bacteria. *Nat. Rev. Microbiol.* **12**, 809-821 (2014).
59. F. Mayer, V. Müller, Adaptations of anaerobic archaea to life under extreme energy limitation. *FEMS Microbiol. Rev.* **38**, 449-472 (2014).
60. F. Kracke, I. Vassilev, J. O. Krömer, Microbial electron transport and energy conservation—the foundation for optimizing bioelectrochemical systems. *Front. Microbiol.* **6**, 575 (2015).
61. A. Gemünde, B. Lai, L. Pause, J. Krömer, D. Holtmann, Redox mediators in microbial electrochemical systems. *ChemElectroChem* **9**, e202200216 (2022).
62. F. Kracke, B. Virdis, P. V. Bernhardt, K. Rabaey, J. O. Krömer, Redox dependent metabolic shift in *Clostridium autoethanogenum* by extracellular electron supply. *Biotechnol. Biofuels* **9**, 249 (2016).
63. E. Marsili *et al.*, *Shewanella* secretes flavins that mediate extracellular electron transfer. *Proc. Natl. Acad. Sci. U.S.A.* **105**, 3968-3973 (2008).
64. K. P. Nevin *et al.*, Electrosynthesis of organic compounds from carbon dioxide is catalyzed by a diversity of acetogenic microorganisms. *Appl. Environ. Microbiol.* **77**, 2882-2886 (2011).
65. Q. Wang, S. Kalathil, C. Pornrunroj, C. D. Sahn, E. Reisner, Bacteria-photocatalyst sheet for sustainable carbon dioxide utilization. *Nat. Catal.* **5**, 633-641 (2022).
66. F. E. Löffler, R. A. Sanford, J. M. Tiedje, Initial characterization of a reductive dehalogenase from *Desulfitobacterium chlororespirans* Co23. *Appl. Environ. Microbiol.* **62**, 3809-3813 (1996).
67. J. He, K. M. Ritalahti, K.-L. Yang, S. S. Koenigsberg, F. E. Löffler, Detoxification of vinyl chloride to ethene coupled to growth of an anaerobic bacterium. *Nature* **424**, 62-65 (2003).
68. R. Sander, Compilation of Henry's law constants (version 4.0) for water as solvent. *Atmospheric Chemistry and Physics* **15**, 4399-4981 (2015).
69. A. F. Schober *et al.*, A two-enzyme adaptive unit within bacterial folate metabolism. *Cell Rep.* **27**, 3359-3370 (2019).
70. L. Wang *et al.*, Peak annotation and verification engine for untargeted LC-MS metabolomics. *Anal. Chem.* **91**, 1838-1846 (2018).
71. J. O. Park *et al.*, Synergistic substrate cofeeding stimulates reductive metabolism. *Nat. Metab.* **1**, 643-651 (2019).
72. M. F. Clasquin, E. Melamud, J. D. Rabinowitz, LC-MS data processing with MAVEN: a metabolomic analysis and visualization engine. *Curr. Protoc. Bioinformatics* **37**, 14.11.11-14.11.23 (2012).
73. M. Kanehisa, Y. Sato, K. Morishima, BlastKOALA and GhostKOALA: KEGG tools for functional characterization of genome and metagenome sequences. *J. Mol. Biol.* **428**, 726-731 (2016).

## Figures and Tables

### A H<sub>2</sub>-mediated materials-biology hybrid for CO<sub>2</sub> fixation

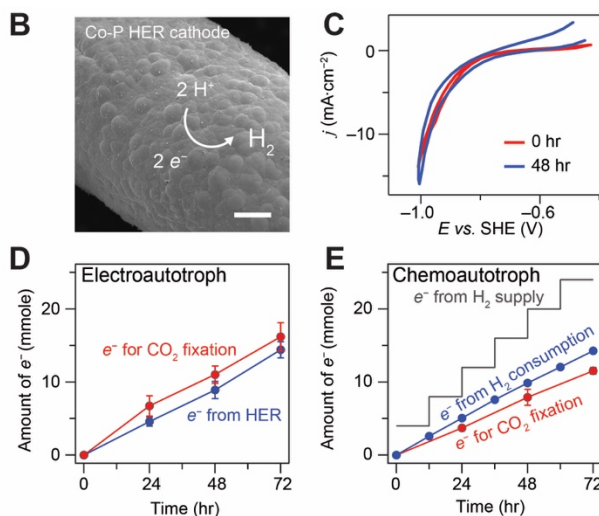
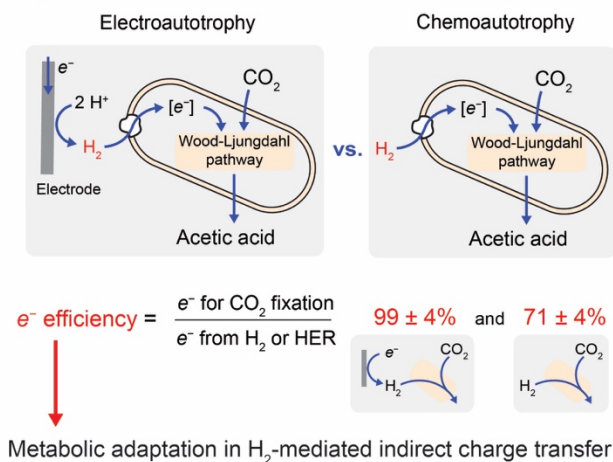


**Figure 1. Enhanced CO<sub>2</sub> fixation in H<sub>2</sub>-mediated materials-biology hybrid.** (A) Schematic comparison of *S. ovata* growth and electron efficiency ( $e^-$  efficiency) under electroautotrophic and chemoautotrophic conditions. (B) Scanning electron microscope image of Co-P alloy cathode for the electrocatalytic hydrogen evolution reaction (HER). Scale bar, 10  $\mu\text{m}$ . (C) Current density-Voltage ( $j$ -V) characteristics of Co-P cathode before and after a 48-hour electrolysis with a scan rate of 50 mV/s in electroautotrophic culture. SHE, standard hydrogen electrode;  $iR$  compensated. (D and E) The amounts of electrons consumption from respective electron donors and recovered from CO<sub>2</sub> fixation in *S. ovata* cultures under electroautotrophic and chemoautotrophic conditions in 72 hours, before correcting for the carryover extracellular nutrients (D and E, and Entry 1 and 3 in the Supplementary Table S1, respectively). The displayed  $e^-$  efficiencies in (A) are the corrected ones after subtracting the carryover extracellular nutrients (see Methods). Data represent biological triplicates ( $n = 3$ , same below). Error bars represent the standard error of the mean (SEM), the same below.

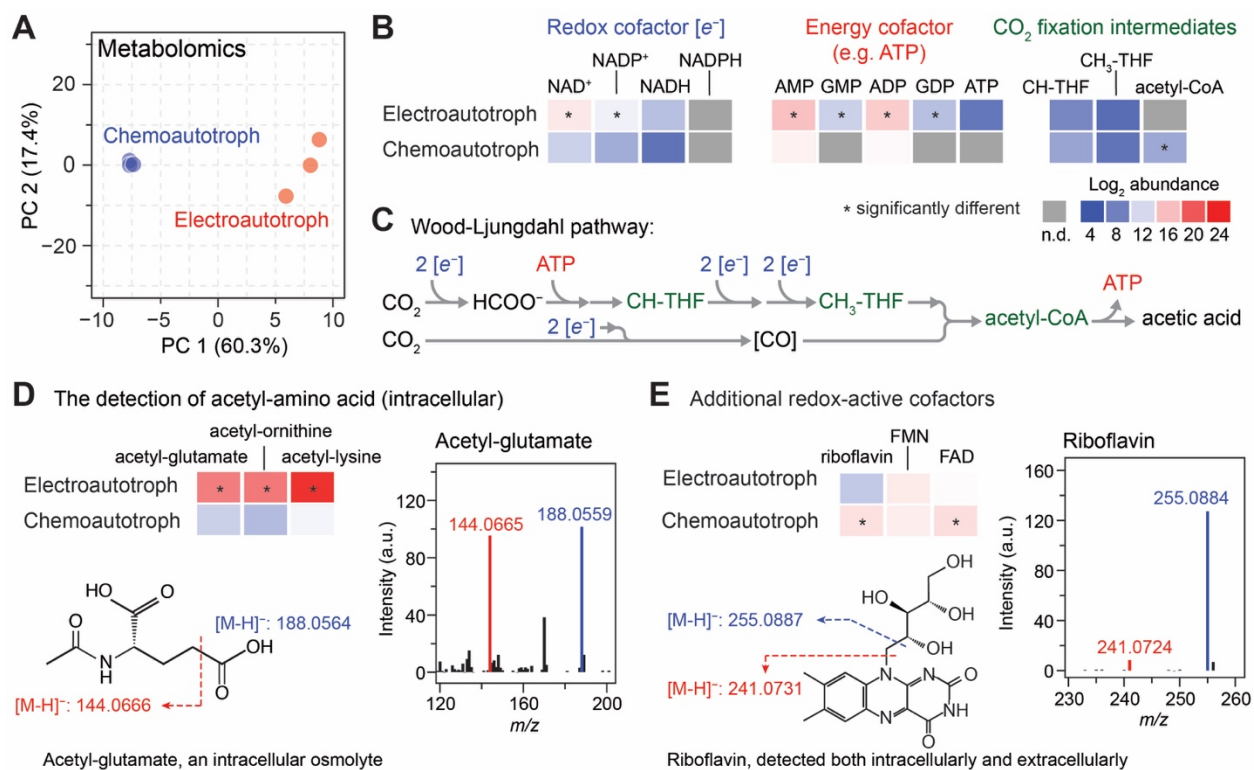


**Figure 2. Metabolomic shift in planktonic *S. ovata* cells induced by electroautotrophy.** (A) The principal component analysis (PCA) of intracellular metabolomes extracted from *S. ovata* cells grown under both electroautotrophic (red) and chemoautotrophic (blue) conditions. Each dot represents one of three biological replicates. (B and C) Heatmaps visualizing abundance changes of metabolites involved in the Wood-Ljungdahl pathway including redox cofactors, energy cofactors and CO<sub>2</sub> fixation intermediates. (D and E) Abundances and tandem mass spectra of intracellular acetyl-glutamate (D) and riboflavin (E). Riboflavin was also detected extracellularly (Supplementary Table S3). Panels (B), (D) and (E) share the same color legend which shown in panel (B). \*, significant difference between conditions (fold change  $\geq 2$  and  $p < 0.05$ ); n.d., not detected; NAD<sup>+</sup> and NADH, Nicotinamide adenine dinucleotide; NADP<sup>+</sup> and NADPH, nicotinamide adenine dinucleotide phosphate; AMP, adenosine monophosphate; GMP, guanosine monophosphate; ADP, adenosine diphosphate; GDP, guanosine diphosphate; ATP, adenosine triphosphate (ATP); CH-THF, methenyl-tetrahydrofolate; CH<sub>3</sub>-THF, methyl-tetrahydrofolate; acetyl-CoA, acetyl coenzyme A; FMN, flavin mononucleotide; FAD, flavin adenine dinucleotide.

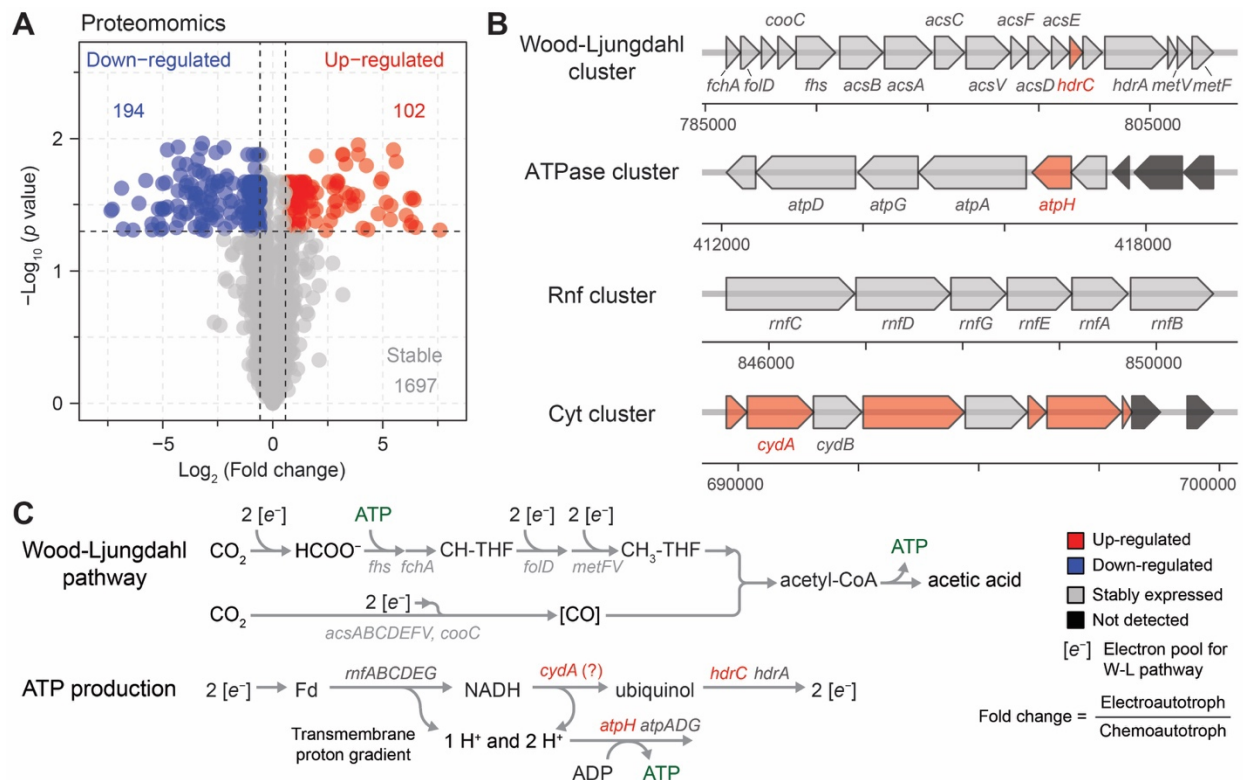
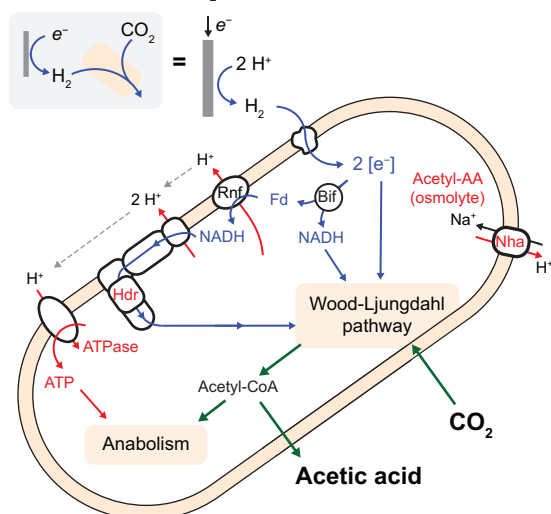


**Figure 3. Electrochemical system induced differential gene expression in *S. ovata* cells.** (A) Volcano plot demonstrating detected proteins in electroautotrophic and chemoautotrophic cells. The differentially expressed proteins were determined by fold change  $\geq 1.5$  and  $p < 0.05$ . The number in color represents the number of proteins determined in the associated category. (B) Expression of gene clusters of interest. The Wood-Ljungdahl cluster includes genes for methenyl-THF cyclohydrolase (*fchA*), methylene-THF dehydrogenase (*folD*), CO dehydrogenase/Acetyl-CoA synthase (*cooC* & *acsABCDEFV*), formyl-THF synthetase (*fhs*), heterodisulfide reductase (*hdrAC*) and methylene-THF reductase (*metFV*) involved in the Wood-Ljungdahl pathway. The ATPase cluster contains genes for ATP synthase (*atpADGH*). The Rnf cluster includes genes encoding ferredoxin:NAD<sup>+</sup> oxidoreductase (*rnfABCDEG*). The Cyt cluster contains genes for cytochrome *bd* (*cydAB*). (C) The involvement of the expressed proteins in the Wood-Ljungdahl pathway and the speculative ATP production pathway. Ferredoxin (Fd).

Metabolic rewiring in H<sub>2</sub>-mediated indirect charge transfer



Electroautotrophy in acetogen: higher  $e^-$  efficiency

**Figure 4. Proposed metabolic rewiring in electroautotrophic *S. ovata*.** The enzymes in black are stably expressed under both electroautotrophic and chemoautotrophic conditions, while the enzymes in red were up-regulated under electroautotrophic conditions. The metabolites in red were more abundant in electroautotrophic cultures. Blue arrows represent electron flow and green arrows represent carbon flow in *S. ovata* metabolism. The proton translocation and ATP synthesis are highlighted by red arrows. Bif, electron-bifurcating hydrogenase; Nha,  $Na^+/H^+$  antiporter; Acetyl-AA, acetyl-amino acids.